Fatigue design of Additive Manufacturing components through Topology Optimization: Comparison of methodologies based on the defect distribution and on the stress gradient

(Article begins on next page)

27 April 2024

ORIGINAL ARTICLE

FFEMS Fatigue & Fracture of Engineering Materials & Structures   WILEY

Fatigue design of Additive Manufacturing components through Topology Optimization: Comparison of methodologies based on the defect distribution and on the stress gradient

Carlo Boursier Niutta [ID] | Andrea Tridello [ID] | Davide S. Paolino [ID]

Department of Mechanical and Aerospace Engineering, Politecnico di Torino, Turin, Italy

Correspondence
Carlo Boursier Niutta, Department of Mechanical and Aerospace Engineering, Politecnico di Torino, Turin, Italy.
Email: carlo.boursier@polito.it

Abstract

In this paper, the fatigue design of AM components is addressed through Topology Optimization. Two defect-driven methodologies, which model the fatigue response in the finite life range and account for the experimental scatter, are compared. The first approach is based on the defect distribution and the marginal P-S-N curves. The second method models the size-effect by accounting for the stress distribution within the loaded material. The two approaches are used to assess the maximum allowable first principal stress, which causes crack propagation. As the fatigue strength depends on the component volume or the stress distribution, an iterative procedure is necessary to determine the optimal design. The optimal topologies of a cantilever beam and of an engine rod are determined and compared, showing that the defect-distribution method is the most conservative and the stress-gradient method can also be reliably applied in the case of uniform stress distribution, as in the engine rod. Furthermore, the choice of the volume to retain for the calculation of the fatigue strength in the defect-distribution method is critical.

KEYWORDS

Additive Manufacturing, defect population, fatigue design, size-effect, Topology Optimization

Highlights

- Fatigue design of additive manufacturing parts through topology optimization.
- Defect-distribution and stress-gradient methodologies for assessing fatigue strength.
- Iterative optimization of cantilever beam and engine rod models.
- The defect-distribution method is the most conservative.
- Stress-gradient and defect-distribution methods converge in uniformly loaded parts.

1 | INTRODUCTION

It is widely known that fatigue represents the most dangerous failure mode for metallic materials, with more than 80% of all in-service failures caused by cyclic loads.[1,2] Among all the factors that affect the fatigue response of components, manufacturing defects randomly distributed within the material volume are one of the most critical. Manufacturing defects act as stress concentrators, enhancing the crack nucleation process[3] and originating fatigue failures even for applied stresses that are considered safe during the design stage. The formation of large defects, for example, is one of the main reasons for the limited diffusion of components produced through Additive Manufacturing (AM) processes. AM processes allow the manufacturing of components with complex shapes with limited manufacturing constraints and material waste compared to traditional subtractive processes.[4,5] For this reason, AM is the most appropriate technique to manufacture components designed with Topology Optimization (TO) processes.[6] TO provides the optimized material distribution to withstand the applied loads.

However, the fatigue performance of AM components is considerably lower than that of traditionally built structures.[7] Indeed, as shown by several works in the literature,[8–11] manufacturing defects typical of AM products,[12] such as pores or cluster of pores, lack of fusion defects, and local microstructural variations, facilitate crack initiation and propagation, thus weakening the fatigue response. Therefore, in the design of AM components, which must sustain fatigue loads, the weakening presence of defects must be properly accounted for.

Fatigue-related TO can be approached by optimizing the fatigue life of the component, that is, the fatigue life is the objective of the TO, or by imposing fatigue constraints within the TO.[13] Holmberg et al.[14] first addressed TO with fatigue constraints. Given a loading history, Holmberg et al.[14] proposed evaluating the maximum allowable fatigue stress through a damage rule and then limiting the first principal stress in the TO. Similarly, Oest and Lund[15] proposed TO where fatigue damage was constrained using Palmgren-Miner's linear accumulation law. More recently, Dagkolu et al.[16] optimized the topology of an aerospace bracket produced by AM. Only static loading conditions were considered in the optimization process, while fatigue loads were accounted in the Finite Element (FE) analysis of the identified TO. As the fatigue performance of AM components strongly depends on the defect distribution, this approach does not guarantee the structural integrity against fatigue, which can be verified only after the

component is produced and the defect distribution is determined, for example, through a micro-CT of the component. Generally speaking, at present, TO and AM cannot be safely employed to design components subjected to fatigue loads, mainly because TO algorithms do not account for the influence of defects on the fatigue response when the component is designed.[13] Fatigue-related TO still has open questions, and some of them will be addressed in this work.

In the last few years, the authors have developed a defect-driven TO design methodology, the so-called Top-Fat methodology. With this approach, the influence of defects is accounted for directly during the TO stage by considering an allowable stress dependent on the defect size distribution. In particular, Murakami's approach and the Statistics of Extremes[3] are exploited to model the influence of defects on the fatigue response. Murakami's formulation provides the fatigue strength starting from the material Vickers hardness, correlated to the material microstructure, and the defect size. On the other hand, by assuming that the defect size follows the Largest Extreme Value Distribution (LEVD), the maximum defect to be expected in the material volume can be reliably estimated. By combining these two factors, an allowable stress, dependent on the defect size and on the loaded volume, is computed to limit the maximum principal stress responsible for the crack propagation.[17] The TopFat methodology has been implemented in a proprietary code[18] and in a commercial code and has been validated on literature benchmarks and a real component used in aerospace applications.[19,20] In the studies of Gao et al. and Boursier Niutta et al.,[18,20] the first principal stress is limited with the computed deterministic fatigue limit, that is, the experimental scatter is not taken into account. However, the experimental scatter can be high, especially when defects are at the origin of fatigue failures[21,22] and cannot be neglected to ensure a safe design and the structural integrity of the component. Moreover, the TopFat methodologies in the studies of Gao et al. and Boursier Niutta et al.[18,20] do not consider the finite fatigue life range, focusing only on the infinite life region. However, depending on the application, a damage-tolerant approach may also be applied to the finite life region. Finally, for a proper application of the TopFat methodology, the distribution of defect size should be reliably known, that is, the parameters of the LEVD should be accurately estimated, for example by analyzing the defect originating the fatigue failure (critical defect, in the following) on the fracture surfaces or through micro-CT analysis. However, the distribution of the defect size may not be available, for example, if the critical defect is not clearly visible on the fracture surface,

thus not allowing for the application of the *TopFat* methodology.

In the present paper, two approaches for defect-driven TO are proposed and numerically investigated. The main difference between the two methods resides in the way the allowable stress and the dependence between the fatigue response and the loaded volume are modeled. The first approach is based on the *TopFat* methodology and on the "marginal P-S-N curves" defined in the study of Paolino et al.[23] Marginal P-S-N curves are P-S-N curves estimated by considering the distribution of defect size and are capable of modeling the fatigue strength variation with the loaded volume. The second methodology models size-effects by considering the distribution of the stress amplitude within the component. Indeed, according to Tridello et al. and Paolino,[24,25] size-effects in defect-driven fatigue response do not depend only on the defect size distribution, but a significant role is played by the stress distribution and the stress gradient within the component. With this second method, therefore, the LEVD parameters are not required as input, and a defect-driven TO can be carried out even if the distribution of defect size is not known. These two approaches are validated with literature benchmarks, starting from material parameters estimated from experimental data obtained by the authors.[26]

2 | METHODS

In this Section, the two methodologies implemented in the defect-driven topology algorithm are recalled and analyzed. Section 2.1 focuses on the method based on the marginal P-S-N curves,[26] whereas Section 2.2 describes the methodology based on the stress gradient.

2.1 | Marginal P-S-N curves

The marginal P-S-N curves are obtained starting from the conditional P-S-N curves, that is, the P-S-N curves conditioned to a specific defect size, and by considering the distribution of defect size. The fatigue life can indeed be seen as a random variable that is conditioned by the applied stress amplitude s_a ($x = \log_{10}[s_a]$) and by the defect size $\sqrt{a_c}$. In the following, the characteristic defect size is assumed as the square root of the area of the defect projected in a direction perpendicular to the maximum applied stress, $\sqrt{a_c}$, according to Murakami.[3] The cumulative distribution function (cdf), $F_Y(y;x)$, of the finite fatigue life $Y = \log_{10}[N_f]$ (being N_f the number of cycles to failure) for an applied stress amplitude equal to s_a ($x = \log_{10}[s_a]$) can be thus expressed as:

$$F_Y(y;x) = \int_0^\infty \Phi\left(\frac{y - \mu_Y(x,\sqrt{a_c})}{\sigma_Y}\right) f_{\sqrt{A_c}}(\sqrt{a_c}) d\sqrt{a_c}, \quad (1)$$

where $\Phi\left(\frac{y-\mu_Y(x,\sqrt{a_c})}{\sigma_Y}\right)$ is the cdf of the conditional finite fatigue life $Y|\sqrt{a_c}$, assumed to follow a normal distribution with a mean $\mu_Y(x,\sqrt{a_c}) = c_Y + m_Y x + n_Y \log_{10}[\sqrt{a_c}]$ and standard deviation σ_Y, and $f_{\sqrt{A_c}}(\sqrt{a_c})$ is the probability density function (pdf) of the defect size $\sqrt{A_c}$, assumed to follow a LEVD with location and scale parameters $\mu_{\sqrt{A}}$ and $\sigma_{\sqrt{A}}$, respectively. The parameters c_Y, m_Y, n_Y, and σ_Y must be estimated from the experimental data (e.g., with a multiple linear regression), whereas the $\mu_{\sqrt{A}}$ and $\sigma_{\sqrt{A}}$ parameters of the LEVD must be estimated from the critical defects $\sqrt{a_c}$ measured on fracture surfaces or through micro-CT analysis. The α-th quantile marginal P-S-N curve can be estimated by solving Equation (1) with respect to x for the range of number of cycles to failure of interest.

The dependency between the fatigue strength and the loaded volume can be obtained by exploiting the properties of the LEVD, according to Equation (2):

$$f_{\sqrt{A_c},T}(\sqrt{a_c}) = T \cdot \left[F_{\sqrt{A_c}}\right]^{T-1} f_{\sqrt{A_c}}(\sqrt{a_c}), \quad (2)$$

where T is the ratio between the volume V for which the fatigue response has to be predicted and the volume of the specimens used for the estimation of the LEVD parameters. For $T = 1$, the fatigue response for the tested specimen volume is obtained. By substituting Equation (2) in Equation (1), the P-S-N curves in function of the loaded volume can be reliably obtained. This model can be implemented in the defect-driven *TopFat* algorithm. The allowable stress, which limits the first principal stress, can be reliably computed from Equations (1) and (2) for the required number of cycles to failure and for the selected volume. Accordingly, for each step of the optimization process, the allowable stress is updated depending on the loaded volume of the component under optimization.

2.2 | P-S-N curves and size effect modelled with the stress gradient

In this section, the stress gradient approach, developed for assessing the allowable stress, is recalled. The fatigue life is assumed to follow a Weibull distribution, and the weakest-link principle is exploited to model the influence on the fatigue response of the stress gradient and the

stress distribution within the component. Accordingly, even if a direct dependency between the fatigue response and the defect size is not modeled, the influence of defects and the variation of the fatigue response and the loaded volume are accounted for. The failure originates from the weakest element; therefore, parts characterized by large volumes of materials subjected to a high-stress amplitude show a lower fatigue response, according to the experimental evidence.

The stress distribution with respect to the material volume represents the necessary input for the application of this methodology. In particular, the distribution of the volumes v_i subjected to a stress amplitude ratio $s_{ratio,i} = \frac{s_i}{s_{max}}$, being s_i a generic stress amplitude and s_{max} the maximum stress amplitude within the part, should be computed. By varying $s_{ratio,i}$ in the range $[0:1]$, the stress ratio distribution for the component can be obtained, for example, with a FE analysis of the component.

According to Invernizzi et al.,[27] an equivalent volume at risk of crack nucleation, v_{eq}, for the analyzed part can be assessed:

$$v_{eq} = \sum_{i=1}^{n_s} v_i s_{ratio,i}^{\gamma}, \qquad (4)$$

where v_i is the material sub-volume subjected to the stress ratio $s_{ratio,i}$, n_s is the number of subdivisions of the stress ratio range (e.g., with $n_s = 100$, $s_{ratio,i}$ is computed with 0.01 steps), and γ is a material parameter to be estimated from the experimental data. Similarly, an equivalent maximum stress amplitude $s_{eq,MAX}$ can be computed by considering the equivalent volume:

$$s_{eq,MAX} = v_{eq}^{\frac{1}{\gamma}} \cdot s_{MAX}. \qquad (5)$$

With $s_{eq,MAX}$, datasets obtained by testing parts with different volumes can be condensed and a master curve can be obtained.[27] Finally, the probability of failure of a component, $F_{N_f}(n; s_{eq,MAX})$, at a number of cycles n and $s_{eq,MAX}$ is expressed by:

$$F_{N_f}(n; s_{eq,MAX}) = 1 - e^{-\left(\frac{n}{\eta_{eq}(s_{eq,MAX})}\right)^{\beta}}, \qquad (6)$$

where β is a material parameter to be estimated from the experimental data, and η_{eq} is defined as:

$$\eta_{eq} = b \cdot s_{eq,MAX}^{k}, \qquad (7)$$

where b and k are material parameters. The model depends on four material parameters, γ, β, b, and k, that must be estimated from the experimental data. By solving Equation (6) with respect to $s_{eq,MAX}$ for the range of n of

interest and by considering $F_{N_f}(n; s_{eq,MAX}) = \alpha$, the α quantile of the master P-S-N curves can be obtained.

This second approach models size-effects starting from the distribution of the stress amplitude in the loaded volume. The allowable stress that must be considered to limit the first principal stress, s_{lim}, can be obtained by expressing Equation (6) as a function of the maximum stress within the part, s_{max}:

$$s_{max} = \left(\ln(1-\alpha)^{-1}\right)^{-1/\beta k} \left(\frac{b \cdot \left(\sum_{i=1}^{n_s} v_i s_{ratio,i}^{\gamma}\right)^{k/\gamma}}{n}\right)^{-1/k}. \qquad (8)$$

From Equation (8), the α quantile of s_{max} at the required n can be computed and considered to limit the first principal stress in TO process.

This method, therefore, does not require estimating the defect size distribution and models the influence of defect size and the variation of the fatigue strength with the loaded volume by exploiting the weakest-link principle. Moreover, the *TopFat* methodology and the approach described in Section 2.1 are dependent on the arbitrary choice of the loaded volume that has to be considered in Equation (2) (volume V). Generally, in the literature, the volume subjected to a stress amplitude above 90% of the maximum applied stress (risk-volume or V_{90}) is considered, according to Murakami,[3] but this choice can also be non-conservative (failures can also occur below the 90% threshold). On the other hand, in[20] described in this section, an arbitrary choice of the volume at risk is not necessary.

2.3 | Integration of fatigue constraint in TO

With reference to the discrete equations of the FE method, the general formulation of a TO problem can be written as:

$$\min_{\overline{\rho}} f(\overline{\rho})$$
$$\text{such that} \quad g_i = \frac{r_i}{l_i} - 1 \le 0 \quad ,$$
$$\text{governed by} \quad \overline{\overline{K}}(\overline{\rho}) \cdot \overline{u} = \overline{F} \qquad (9)$$
$$\text{where} \quad \overline{\rho} = \{\rho_1, \rho_2, ..., \rho_N\}$$

where f is the objective function to minimize, for example, the mass or the global compliance of the component, g_i is the i-th constraint function, with r_i the response of the system and l_i the corresponding limit state, $\overline{\rho}$ is the

vector of design variables, that is, the relative densities of the N elements, $\bar{\bar{K}}$ is the stiffness matrix, which depends on the relative densities, $\bar{u}$ is the displacement vector, and $\bar{F}$ is the external force vector. In the following, two stress constraint functions will be considered. Firstly, a constraint for the static loading condition limits the Von Mises stress of each element to be at most equal to the yield strength of the material. Secondly, a constraint for the fatigue loading conditions is considered, with the first principal stress limited by the maximum allowable stress calculated according to the approaches described in Sections 2.1 and 2.2.

For the defect-distribution approach, the maximum allowable stress depends on the size of the most critical defect, which in turn depends on the volume of the component (see Equation 2). As in TO, the volume changes at each iteration, an iterative procedure is necessary.[20]

In the stress-gradient approach, according to Equation (8), the maximum allowable fatigue stress depends on the stress distribution within the loaded material. The stress field depends on the final topology of the component. Therefore, an iterative procedure is also necessary for the stress-gradient approach.

Figure 1 shows a flowchart of the iterative procedure here adopted to identify the optimal topology.
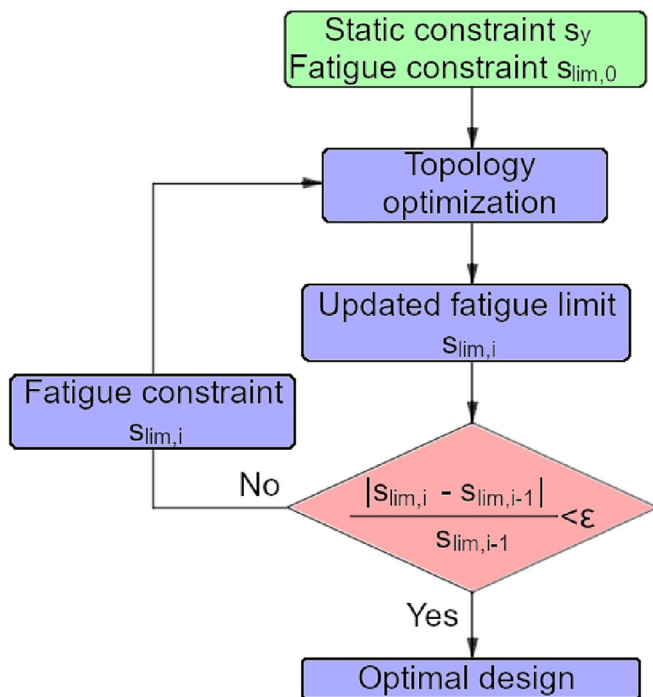

FIGURE 1 Flow chart of the iterative topology optimization (TO) with fatigue constraint. [Colour figure can be viewed at wileyonlinelibrary.com]

In the first run, the first principal stress of each element is limited by a maximum allowable stress $s_{lim,0}$, which is calculated:

a. For the defect-distribution approach, from the initial volume V_0 of the component, that is, the initial volume of the whole design domain (see Equations 1 and 2),

b. For the stress-gradient approach, from the stress distribution (see Equation 8). Therefore, in the stress-gradient approach, a preliminary FE analysis is necessary in order to assess the first principal stress and the volume of each element of the model.

The resulting topology of the component has a volume V_{opt}, depending on the retained threshold for the relative densities. Indeed, at the end of the optimization process, the relative density of each element is comprised between 0, that is, the element can be completely removed, and 1, that is, the element is necessary to sustain the load. The designer is thus requested to choose if elements with intermediate densities are to be considered or can be excluded. In this work, a threshold value of 0.4 has been considered for the identification of the resulting topology, in accordance with the study of Boursier Niutta et al.[20]

An updated value of the maximum allowable stress $s_{lim,i}$ can thus be calculated according to the adopted approach (Equations 1 and 2 or Equation 8) and compared to the value used in the optimization process. If the difference is sufficiently small, it can be assumed that the obtained topology is no longer affected by the slight change in the fatigue stress constraint, and the process is stopped. The convergence criterion is met when the discrepancy between the updated maximum allowable stress $s_{lim,i}$ and that used in the optimization process $s_{lim,i-1}$ is smaller than an ε value, for example, 1%. On the contrary, when the difference between the updated maximum allowable stress $s_{lim,i}$ and that computed by the optimization algorithm is still consistent, that is, the discrepancy is greater than the convergence criterion, another TO is run by limiting the first principal stress with $s_{lim,i}$. The process thus iteratively proceeds until the convergence criterion is met.

Regardless of the approach considered for the calculation of the fatigue strength, the iterative procedure can be adopted even when volume constraints are imposed (e.g., the final topology must have at most 50% of the initial volume). In the case of the stress-gradient approach, the iterative procedure is still necessary when volume constraints are imposed, since the stress distribution and so the fatigue constraint vary with the topology of the

component; whereas, in the case of the defect-distribution approach, the maximum allowable stress can be calculated straightforwardly from the imposed limit on the volume, avoiding the iterative procedure.

Furthermore, it is worth noticing that, when the fatigue constraint is imposed according to the defect-distribution approach, it is assumed that the largest defect is present in each element of the FE model. Indeed, in the TO process, the first principal stress of each element of the FE model is limited by the maximum allowable first principal stress s_{lim}, which is determined as a function of the largest defect $\sqrt{a_c}$ through Equations (1) and (2). This assumption, which also allows to consistently simplify the TO process, can be too conservative. In place of the whole volume of the optimized component, the designer can consider the volume that experiences a limited range of stress amplitudes. For example, the volume of material that is loaded at least by 90% of the maximum applied stress, the V_{90}, can be considered for the calculation of the maximum allowable stress with the defect-distribution approach.[3] However, the arbitrary choice of the retained volume consistently affects the final topology and the iterative process, as will be shown in the next section.

3 | NUMERICAL VALIDATION

In this section, the proposed methodologies are validated with literature benchmarks, starting from experimental data on AlSi10Mg alloy collected by the authors.[26] Two mechanical components are considered: a cantilever beam and an engine rod, both subjected to static and fatigue loading conditions. In the cantilever beam problem, the compliance of the structure is minimized. Instead, the engine rod is optimized in order to minimize its mass while guaranteeing structural strength. The optimizations are run with the commercial software *Hypermesh*, which operates with an algorithm based on the dual method.[28]

The section is organized as follows: in Section 3.1, the experimental results are analyzed to estimate the models for the estimation of the allowable stress; in Section 3.2, the cantilever beam model is presented and optimized both with the defect-distribution and with the stress-gradient approach; and finally, in Section 3.3, the engine rod problem is addressed with the two methods.

3.1 | Models estimation for the calculation of the fatigue constraint

For the validation of the proposed methodologies, the experimental results obtained by the authors in the study

of Tridello et al.[26] are considered. In the study of Tridello et al.,[26] size-effects on the fatigue response up to 10^9 cycles of AlSi10Mg alloy specimens produced through a selective laser melting (SLM) process have been investigated. Experimental tests on hourglass specimens, characterized by a risk volume V_{90} of $200 \, mm^3$, and on Gaussian specimens,[29] with a risk volume V_{90} of $2300 \, mm^3$, have been carried out on specimens built in horizontal and vertical directions. The fracture surfaces of the specimens have been observed with a scanning electron microscope (SEM) to investigate the failure's origin. All the fatigue failures have been found to originate from manufacturing defects, typical of SLM processes, like pores and a lack of fusion defects. In the following, the experimental results obtained by testing the AlSi10Mg specimens built in horizontal direction are considered.

The marginal P-S-N curves are estimated by considering the experimental results obtained through tests on hourglass and Gaussian specimens together. As described in Section 2.1, the fatigue life, conditioned to the critical defect, is assumed to follow a normal distribution with a mean μ_Y and a standard deviation σ_Y. The mean is expressed as a function of the stress amplitude, $x = \log_{10}[s_a]$, and of the critical defect, $\sqrt{a_c}$, by $\mu_Y(x, \sqrt{a_c}) = c_Y + m_Y x + n_Y \log_{10}[\sqrt{a_c}]$, with the parameters c_Y, m_Y, and n_Y estimated from the experimental data. The standard deviation σ_Y is assumed to be constant and is also determined from the experimental data. The LEVD parameters of the critical defect distribution are estimated starting from all the $\sqrt{a_c}$ measured on the fracture surfaces of the tested specimens, regardless of the specimen type, by exploiting the LEVD properties, according to Equation (2). Moreover, the local stress amplitude s_{local}, that is, the stress amplitude computed at the defect location, is considered in place of the stress at the specimen center. Indeed, as the experimental campaign conducted in the study of Tridello et al.[26] investigated the fatigue response of the material through ultrasonic tests and the stress field within the specimen is not constant, the stress in correspondence of the critical defect, that is, s_{local}, must be considered in order to properly determine the marginal P-S-N curves.

The P-S-N curves dependent on the stress gradient are estimated by considering the experimental results obtained by testing the hourglass and the Gaussian specimens, according to Invernizzi et al.[27] Considering the stress distribution within specimens, for example, obtained through an FE element, the specimen is divided into uniformly stressed sub-volumes. According to the approach described in Section 2.2, the fatigue life of each sub-volume is a random variable assumed to follow a Weibull distribution and is related to the stress amplitude

according to Basquin's model. The fatigue life of the specimen is finally obtained from the fatigue lives of the sub-volumes through the weakest link principle. The stress at the specimen center is considered in this case since this method can be applied without knowing the crack origin site.

Figure 2 shows the experimental data of the hourglass and the Gaussian specimen, together with the estimated median and the 0.1-th quantile P-S-N curves: Figure 2A shows the marginal P-S-N curves, whereas Figure 2B shows the P-S-N curve estimated by considering the stress gradient. In Figure 2A, the 0.1-th quantile P-S-N curve for hourglass specimens is not clearly visible since it is partially hidden by the median P-S-N curve for Gaussian specimens. In this paper, the fatigue strength for the TO has been calculated at 10^9 cycles.

3.2 | Cantilever beam

In this section, the cantilever beam is optimized by minimizing its compliance while guaranteeing its structural strength. A constraint on the volume is also considered. The optimization is performed first by considering the fatigue constraint calculated through the defect-distribution approach and then retaining the fatigue strength calculated through the stress-gradient method.

3.2.1 | Mechanical model

Figure 3 shows the geometry and dimensions of the cantilever beam subjected to TO.

The beam has a thickness of 3 mm, and 2D four-node elements are considered for discretizing the structure. A

mesh size of 1 mm is adopted, thus leading to a total of 15,000 elements.

The degrees of freedom of the nodes in correspondence of the clamped cross-section are constrained, while the external force is distributed over 11 neighboring nodes to avoid stress concentration.

Two loading conditions are considered: one simulating the static case, with the external load equal to 1.5 kN, and one for the fatigue case, with the external force equal to 1 kN. In the *Hypermesh* environment, two load step identities can be defined, one for each loading condition. At each iteration of the optimization process, two linear static analyses are performed: one with the maximum loading conditions, that is, those for the static verification, and one with the fatigue loading case.

The material of the cantilever beam is the as-built AlSi10Mg, the same used in the study of Tridello et al.[30] The Young's modulus is 70 GPa, the material density is 2.69 g/cm^3, and the yield strength is 287 MPa.

3.2.2 | Structural-mechanical problem

The compliance of the structure is minimized, while the structural strength is guaranteed against static and fatigue loads. A volume constraint is also considered, that is, the total volume of the optimized component is 40% of the initial volume. As the final volume is imposed, the maximum allowable stress according to the defect-distribution approach can be directly calculated, and the optimization can be run without the iterative procedure. The optimization problem based on the defect-distribution method can thus be written as:
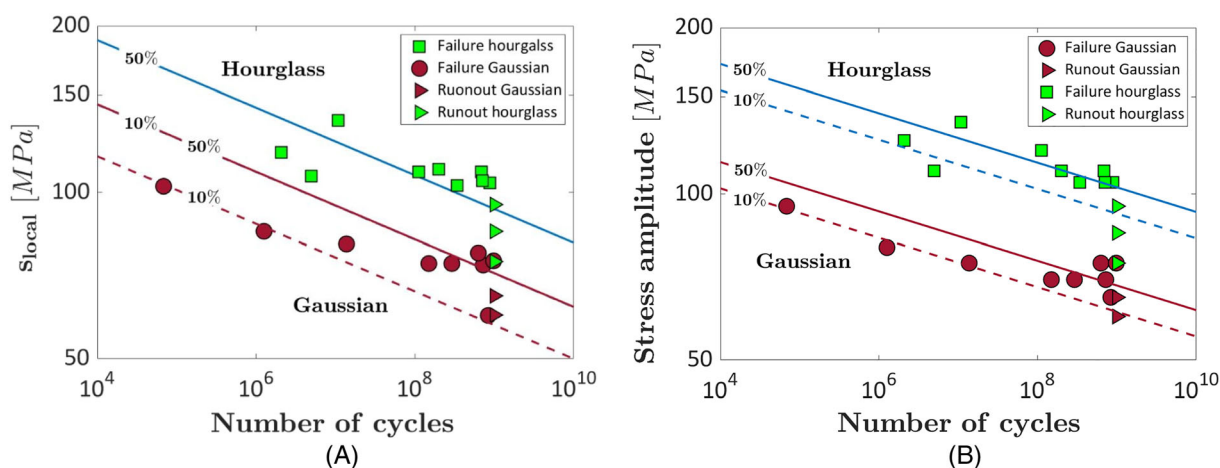

FIGURE 2 P-S-N curves for ALSi10Mg alloy were estimated with the two investigated methodologies: (A) marginal P-S-N curves; (B) P-S-N with the stress gradient approach. [Colour figure can be viewed at wileyonlinelibrary.com]
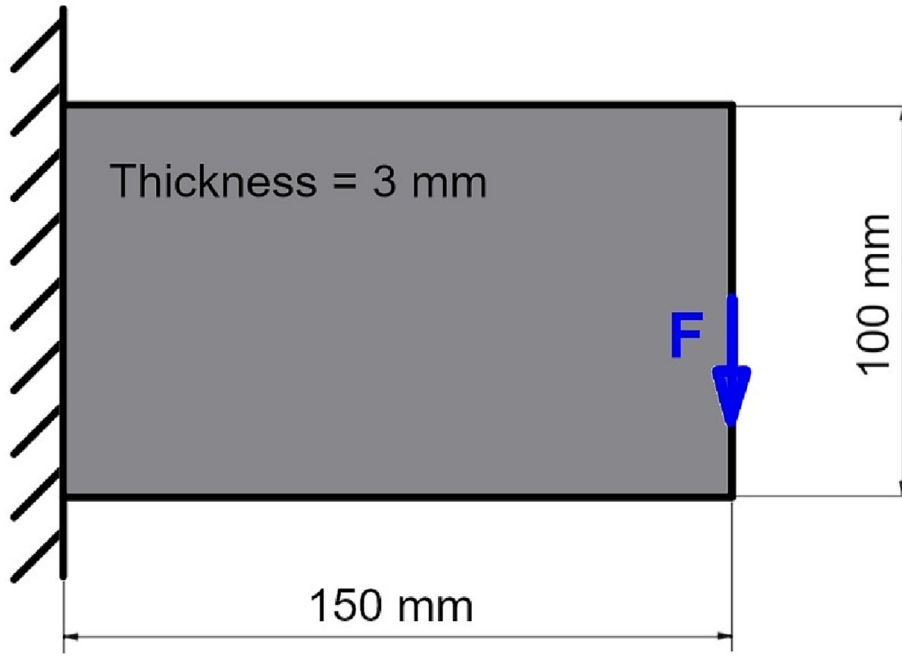
$$\min_{\overline{\rho}} C(\overline{\rho})$$

$$\text{such that} \quad g_1 = \frac{V_{opt}}{0.4 \cdot V_0} - 1 \le 0$$

$$g_2 = \frac{s_{eq}}{s_y} - 1 \le 0 \qquad (10)$$

$$g_3 = \frac{s_1}{s_{lim}} - 1 \le 0$$

$$\text{governed by} \quad \overline{\overline{K}}(\overline{\rho}) \cdot \overline{u} = \overline{F}$$

$$\text{where} \quad \overline{\rho} = \{\rho_1, \rho_2, ..., \rho_N\}$$

where C is the total compliance of the cantilever beam calculated from the maximum displacement, V_0 the initial volume of the cantilever beam, that is, 45,000 mm³, V_{opt} is the volume of the optimal design, that is, 18,000 mm³, s_{eq} is the Von Mises stress of each element, s_y is the static limit, that is, the yield strength of the material, s_1 is the first principal stress of each element, and s_{lim} is the maximum allowable stress, which results equal to 50 MPa according to the defect-distribution method, being $V_{opt} = 18000mm3$.

The stress-gradient approach instead requires an iterative procedure as the stress field depends on the topology of the component. A preliminary FE analysis is performed to assess the initial value of the maximum allowable principal stress $s_{lim,0}$. The maximum allowable stress is then updated once the optimization is complete and the stress distribution can be determined. In particular, at the end of the optimization process, elements with a relative density smaller than 0.4 are deleted, and a FE re-analysis of the optimal topology is performed for the determination of the stress within each element.

The optimization problem based on the stress-gradient approach is thus formulated as:

$$\text{while} \quad \frac{|s_{lim,i} - s_{lim,i-1}|}{s_{lim,i-1}} > 0.01$$

$$\min_{\overline{\rho}} C(\overline{\rho})$$

$$\text{such that} \quad g_1 = \frac{V_{opt}}{0.4 \cdot V_0} - 1 \le 0$$

$$g_2 = \frac{s_{eq}}{s_y} - 1 \le 0 \qquad (11)$$

$$g_3 = \frac{s_1}{s_{lim,i-1}} - 1 \le 0$$

$$\text{governed by} \quad \overline{\overline{K}}(\overline{\rho}) \cdot \overline{u} = \overline{F}$$

$$\text{where} \quad \overline{\rho} = \{\rho_1, \rho_2, ..., \rho_N\}$$

where $s_{lim,i-1}$ is the maximum allowable stress at the i-th optimization run and $s_{lim,i}$ is the updated value at the end of the optimization run. Although the optimization formulation is the same as reported in Equation (11), Equation (10) highlights the iterative procedure required by the stress-gradient method. The iterative procedure ends when the discrepancy between $s_{lim,i}$ and $s_{lim,i-1}$ is smaller than 1%.

3.2.3 | Results and discussion

The results of the TOs of the cantilever beam are summarized in Table 1, while Figure 4 shows the optimal topologies and contour plots of the first principal stress obtained with the two methods.

TABLE 1 Results of the TOs of the engine rod for the different methods.

Formulation	Global compliance (mm·N^{-1})	Mass of optimal design (g0	Optimization runs (iterations within each run)	Total computational time (s)	Fatigue constraint $s_{lim,i}$ (MPa)
Defect-distribution	118.9	51.4	1 (45)	200	50.0
Stress-gradient	103.0	49.9	3 (95 + 44 + 42)	900	100–121.4–132

Abbreviation: TO, topology optimization.
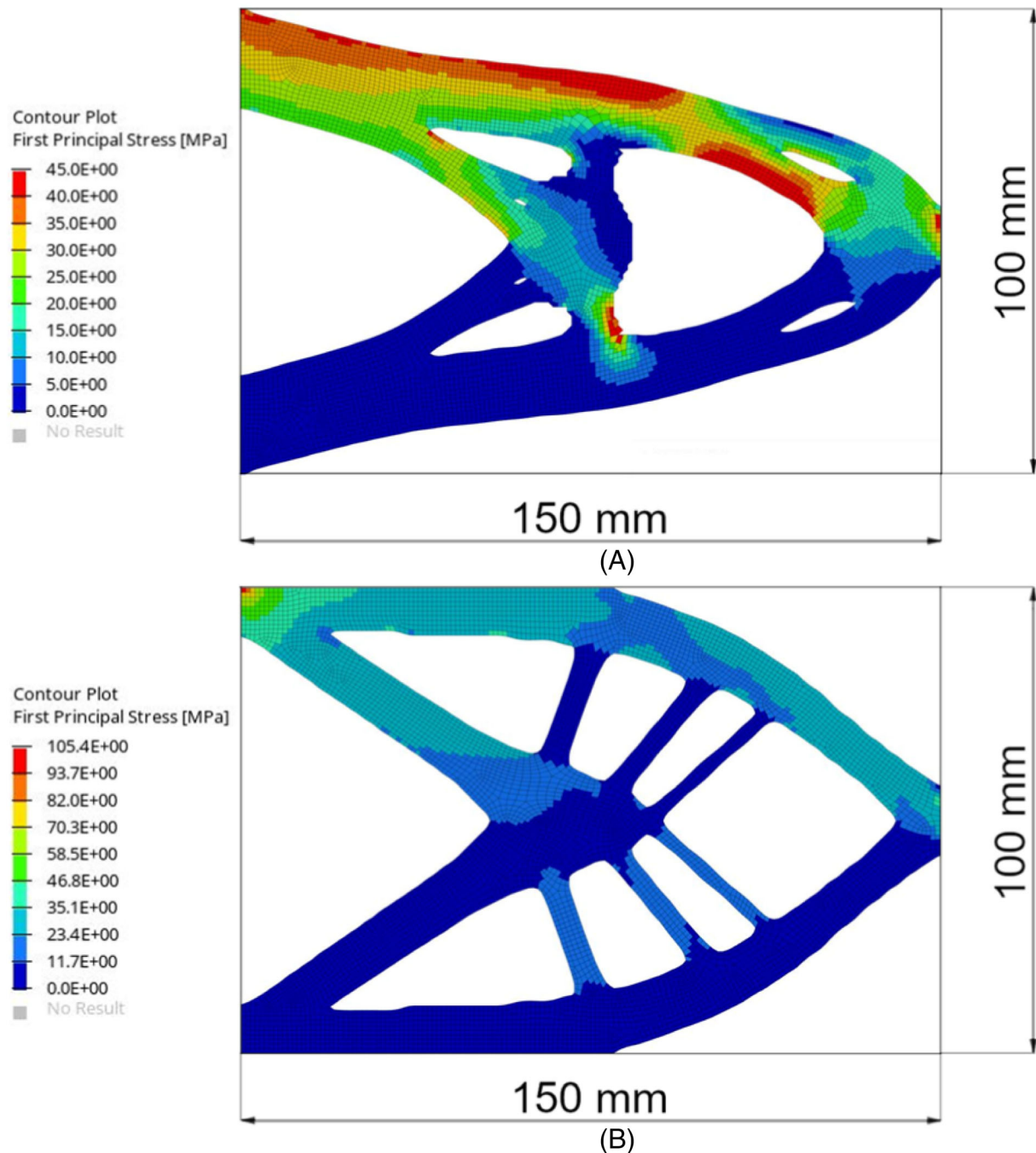
FIGURE 4 Topologies and contour plots of the first principal stress: (A) defect-distribution based optimization; (B) stress-gradient based optimization. [Colour figure can be viewed at wileyonlinelibrary.com]

According to Table 1, the mass of the optimal designs is almost the same given the volume constraint retained in the optimization formulation, while the global compliance of the structure, the final topologies, and the stress distributions of the first principal stress are consistently different.

In the defect-distribution approach, the maximum allowable stress is equal to 50 MPa, less than half of the value obtained through the stress-gradient method. The defect-distribution approach indeed assumes that the largest defect is equivalently present in all the elements of the FE model, which represents a conservative assumption. In order to meet this restrictive constraint, the topology of the cantilever beam is tapered at the expense of the global compliance.

In the stress-gradient approach, the maximum allowable stress depends on the stress distribution within the component. The bigger the material volume loaded at a high stress level, the lower the fatigue strength, according to the weakest-link principle. In the cantilever beam model, few elements are highly loaded (those in correspondence of the clamped cross-section), as also shown in Figure 5, where uniformly stressed sub-volumes of the cantilever beam obtained at the end of each optimization run are reported.

According to Figure 4 and Table 1, the maximum allowable stress is consistently higher than that calculated with the defect-distribution approach. In this regard, it is worth noticing that, as the fatigue loading conditions assume a stress ratio R = −1 and given the

symmetry of the problem, the volume of the elements subjected to a given stress ratio has been doubled in order to take into account that both the upper and lower parts of the beam are subjected to positive tensile stress from which the crack can propagate.

As shown in Figure 5, very sparse volumes are subjected to a high stress level while most of the material experiences intermediate or low stress ratio levels, being the stress ratio defined as $s_{ratio} = \frac{s}{s_{max}}$, where s is the first principal stress in the element or sub-volume and s_{max} is the maximum value of the first principal stress in the part, in accordance with Equation (8). As a consequence, high fatigue strength is admitted for the component.

Furthermore, the stress-gradient method requires some optimization runs (three in the present case study) to converge to the optimal design, in addition to the preliminary FE analysis necessary to evaluate the initial stress field. The computational effort is thus consistently higher with respect to the defect-distribution approach. As shown in Table 1, the computational time required to achieve the optimal topology through the stress-gradient based formulation is about 4 times higher than that required by the defect-based formulation. For the computational effort, it is worth mentioning that, at each iteration of the optimization problem, the software performs an elastic FE analysis. Thereafter, the topology is updated by modifying the density of each element of the model according to the optimization algorithm. The time required by each iteration is mainly related to the FE
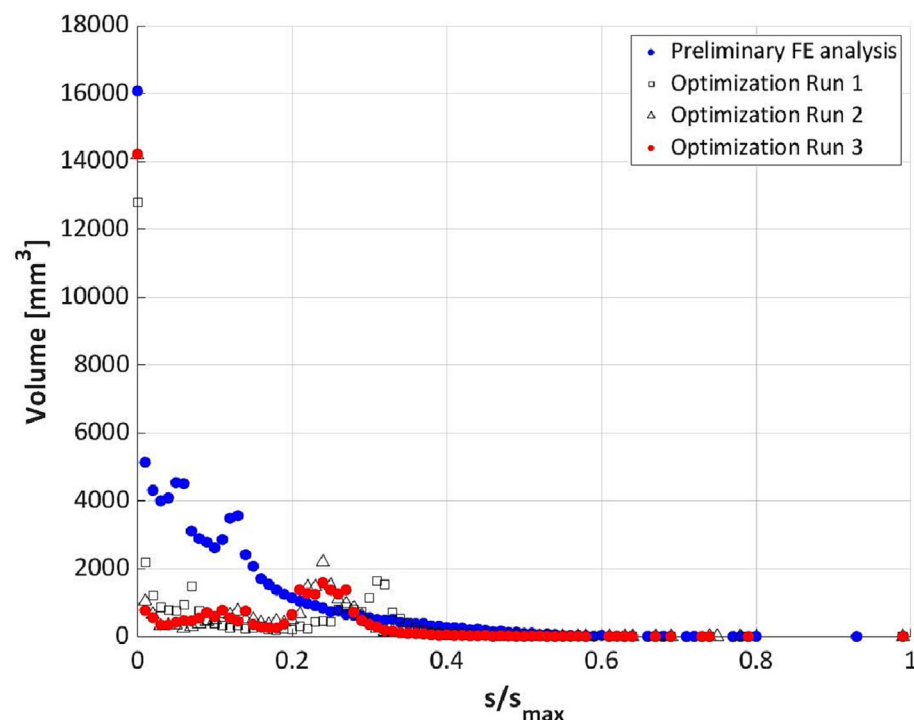

FIGURE 5 Uniformly stressed sub-volumes of the cantilever beam after each optimization run. [Colour figure can be viewed at wileyonlinelibrary.com]

analysis, which lasts 5 s on average on a desktop computer with an Intel Core i7-8700 (3.2 GHz) and 32 GB of RAM.

Finally, in regard to the static loading condition, both optimal designs can sustain the load with remarkable differences with respect to the ultimate strength of the material. In particular, the cantilever beam obtained with the defect-distribution approach shows a maximum Von Mises stress of about 75 MPa, while in the cantilever beam obtained with the stress-gradient method, the maximum Von Mises stress is equal to almost 170 MPa. Both values are consistently smaller than the yield strength of the material, which is 287 MPa.

3.3 | Engine rod

This section addresses the engine rod model, who's mass is minimized, while the structural constraints on the static and fatigue loading conditions are retained. Both methods are employed. For the defect-distribution approach, the optimization is run both by considering the whole component volume and the volume that experiences at least 90% of the maximum applied stress, as suggested in the study of Murakami.[3]

3.3.1 | Mechanical model

Figure 6 reports the geometry data of the engine rod. Design and non-design domains are highlighted in gray and red, respectively.

According to Figure 6, the regions in correspondence of the bushings are non-design domain in order to guarantee the correct mounting of the engine rod on the crankshaft. From the results of a mesh convergence study, the engine rod has been discretized with 18,163 tetra-elements, with a maximum element size of 2 mm.

The engine rod of a four-stroke engine experiences tensile and compressive loads within the 720° of rotation of the crankshaft, which is necessary to complete a cycle. The maximum compressive load is encountered in correspondence of the engine combustion, while the maximum tensile load corresponds to the maximum acceleration experienced by the engine rod, which occurs in the exhaust phase. The two loading cases are usually slightly different[31] and, for simplicity, are here assumed equal, leading to a stress ratio R = −1. In particular, as the topology can be affected by the direction of the external load, the tensile loading condition is retained in the FE analysis as shown in Figure 6, given that the crack propagates when the rod experiences the tensile load.

In the static loading case, which corresponds to an overload condition and is encountered at the maximum power of the engine, the engine rod is loaded by 25 kN. In the regime condition, which can be retained for the fatigue design, an external load of 15 kN is assumed. As for the cantilever beam, two load step identities are defined in *Hypermesh*, and the software performs two linear elastic analyses at each iteration of the optimization process.

The connection with the pin of the piston and with the crankshaft is modeled through rigid elements (RBE2
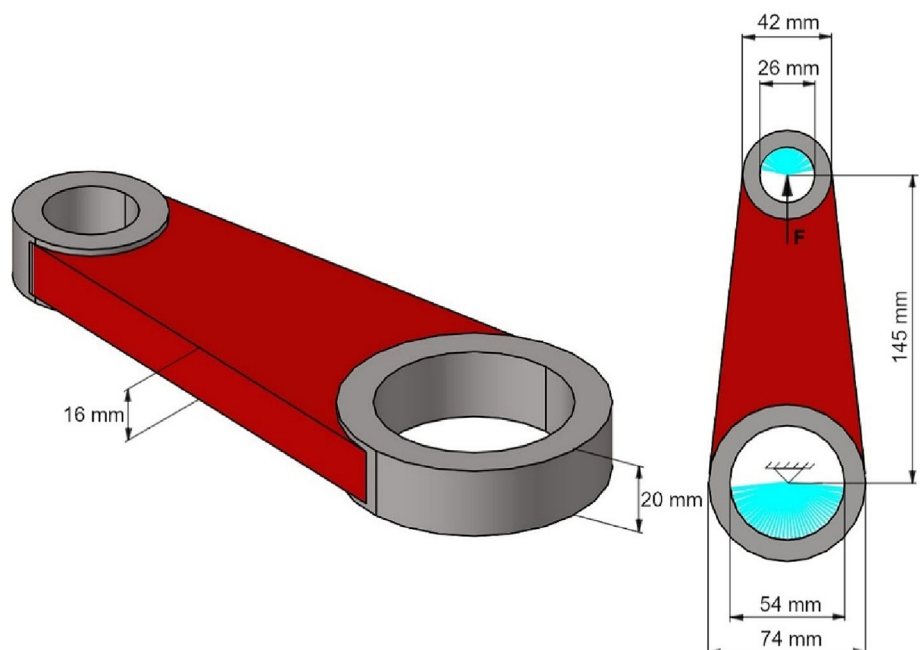

FIGURE 6 Design domain (in red) and non-design domain (in gray) of the engine rod. [Colour figure can be viewed at wileyonlinelibrary.com]

elements in *Hypermesh*), represented by the blue lines in Figure 6. The load transmitted from the pin of the piston to the engine rod is applied to a central node and transferred to the engine rod by means of the rigid elements. In correspondence of the bottom bushing, a central node connected to the engine rod through rigid elements is fully constrained in order to simulate the constraint provided by the crankshaft.

The material of the engine rod is the as-built AlSi10Mg, the same as used in cantilever beam.

3.3.2 | Structural-mechanical problem

The mass of the engine rod is minimized, while only static and fatigue constraints are considered. Both methods require the iterative procedure shown in Figure 1 to complete the optimization, which is thus formulated as:

$$
\begin{aligned}
\text{while} \quad & \frac{|s_{lim,i} - s_{lim,i-1}|}{s_{lim,i-1}} > 0.01 \\
& \min_{\overline{\rho}} m(\overline{\rho}) \\
\text{such that} \quad & g_1 = \frac{s_{eq}}{s_y} - 1 \leq 0 \\
& g_2 = \frac{s_1}{s_{lim,i-1}} - 1 \leq 0 \\
\text{governed by} \quad & \overline{\overline{K}}(\overline{\rho}) \cdot \overline{u} = \overline{F} \\
\text{where} \quad & \overline{\rho} = \{\rho_1, \rho_2, ..., \rho_N\}
\end{aligned}
\tag{12}
$$

where m is the mass of the component, s_{eq} is the Von Mises stress of each element, s_y is the static limit, that is, the yield strength of the material, s_1 is the first principal stress of each element, $s_{lim,i-1}$ is the maximum allowable stress at the i-th optimization run, and $s_{lim,i}$ is the updated value at the end of the optimization process. The iterative procedure ends when the discrepancy between $s_{lim,i}$ and $s_{lim,i-1}$ is smaller than 1% for both approaches.

In order to show that the choice of the adopted volume consistently affects the final topology and the iterative process, two optimizations based on the defect-distribution approach have been performed. In the first, the maximum allowable value $s_{lim,i}$ of the fatigue constraint has been calculated based on the total volume resulting at the end of an optimization run. In the second, the maximum stress $s_{lim,i}$ of the fatigue constraint has been calculated considering V_{90}, that is, the volume of material that is loaded at least by 90% of the maximum applied stress.

3.3.3 | Results and discussion

Results of the optimization are reported in Table 2 for the different methods.

According to Table 2, the mass of the optimal topology and the iterative procedure are strongly influenced by the retained approach. The defect-distribution approach, which considers the total volume V_{tot} at the end of the optimization run, leads to results similar to those obtained through the stress-gradient method.

As in the case of the cantilever beam, the higher mass of the component optimized with the defect-distribution approach can be explained by considering that this method assumes that the largest defect is equivalently present in all the elements of the component, which represents a conservative assumption.

Regarding the stress-gradient method, Figure 7 reports the distribution of uniformly stressed volumes within the loaded material at the end of each optimization run. In particular, uniformly stressed sub-volumes of material are considered with respect to the stress ratio $s_{ratio} = \frac{s}{s_{max}}$, where s is the first principal stress and s_{max} is the maximum value within the part.

As can be noticed from Figure 7, unlike in the cantilever beam case, where only a few elements experienced the highest stress, the load distribution is more uniform in the engine rod, that is, consistent volumes of material

TABLE 2 Results of the TOs of the engine rod for the different methods.

Formulation	Mass of optimal design (g)	Optimization runs (iterations within each run)	Total computational time (s)	Fatigue constraint $s_{lim,i}$ (MPa)
Defect-distribution V_{tot}	168.8	2 (45 + 48)	500	45.7–46.6
Defect-distribution V_{90}	120.0	5 (45 + 51 + 58 + 93 + 60)	1600	45.7–71.6–102.8–83.4–80.4
Stress-gradient	162.1	4 (76 + 52 + 60 + 46)	1100	76–55.5–48.3–49.6

Abbreviation: TO, topology optimization.

FIGURE 7 Uniformly stressed sub-volumes of the engine rod after each optimization run. [Colour figure can be viewed at wileyonlinelibrary.com]
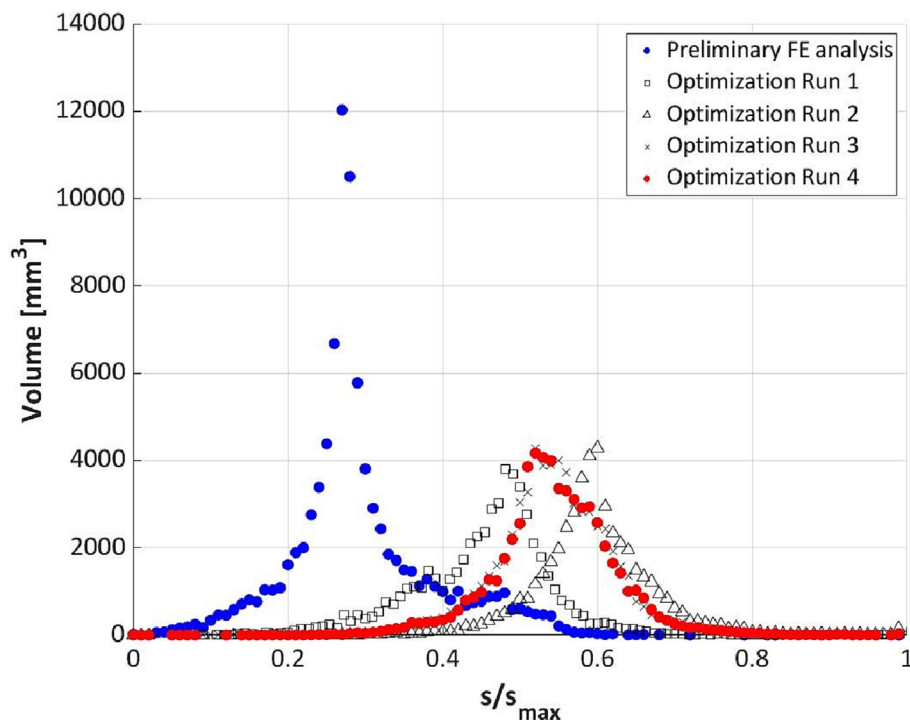
are subjected to high stress ratio levels. As a consequence, in the engine rod, the fatigue strength admitted for the part through the stress-gradient method approximates the conservative value obtained through the defect-distribution approach with V_{tot}.

The defect-distribution approach with total volume V_{tot} and the stress-gradient approach mainly differ in the number of optimizations required to reach convergence in the iterative procedure. In the stress-gradient approach, fatigue strength depends on the stress distribution within the part. As shown in Figure 7, the stress distribution varies in the first three optimizations, while at the fourth iteration, the stress field affects almost the same amount of material as in the third optimization run, confirming that convergence is imminent. Indeed, at the end of the fourth optimization, the maximum allowable stress $s_{lim,i}$ resulted equal to 49.9 MPa, and the discrepancy with respect to the $s_{lim,i-1}$ value of 49.6 MPa is lower than 1%. The slight oscillations of the maximum allowable stress $s_{lim,i}$ before convergence are reached can also be appreciated in Figure 7, where the stress ratio level, which loads most of the material, goes back and forth. In total, the optimization problem required 1100 s to achieve the optimal topology on the desktop computer with an Intel Core i7-8700 (3.2 GHz) and 32 GB of RAM, as shown in Table 2.

On the contrary, the defect-distribution approach, which considers the total volume at the end of the optimization run, more rapidly converges to the optimal design. The time required to complete the optimization

was about 500 s, less than half of the time required through the formulation based on the stress-gradient method. The maximum allowable stress $s_{lim,i}$ depends on the total volume of the topology, and in the defect-distribution approach, the relationship is governed by LEVD distribution parameters. At high volumes, the variation of $s_{lim,i}$ with the volume is limited, thus leading to a fast convergence. For the engine rod, the initial volume of the design domain is equal to 90,000 mm³, while the volume of optimal design is almost equal to 63,000 mm³. According to the retained material, the process can require further optimization runs.[20] On the contrary, at low volumes, that is, at volumes comparable with those of the tested specimen, the maximum allowable stress is strongly sensitive to volume variations.

This can be appreciated by considering the results of the defect-distribution method, where only the V_{90}, that is, the volume that experiences at least 90% of the maximum stress, is considered. The maximum allowable stress $s_{lim,i}$ strongly oscillates, and several optimizations are required to reach convergence. The total time required to achieve the optimal topology was about 1600 s, which is much higher than the other formulations, as shown in Table 2.

The topologies of the optimal design are reported in Figure 8, where the contour plots of the first principal stress are represented for the design domain region.

The topologies are all symmetric with respect to the main axis of the rod. As observed in Table 2, the topologies based on the defect-distribution approach with V_{tot}

and on the stress-gradient method are similar. On the contrary, the topology of the defect-distribution approach, which considers only the V_{90}, is consistently different from that obtained considering the total volume in the calculation of the maximum allowable stress.

The stress contour plots in Figure 8 also show that the elements experiencing the maximum allowable stress are limited in all the topologies. In particular, the volume subjected to at least 90% of the maximum stress is 136.2 mm^3 in the defect-distribution approach with V_{tot} ($s_{lim,i} = 46.6$ MPa), 67.9 mm^3 in the defect-distribution approach with V_{90} ($s_{lim,i} = 80.4$ MPa) and 79.2 mm^3 ($s_{lim,i} = 49.9$ MPa). With reference to the defect-distribution approach, as the volume of material loaded by the maximum stress is limited, the assumption for

which the largest defect is equivalently present in all the elements is not strongly restrictive.

As a general comment, the results reported in Table 2 and in Figure 8 show that the choice of the retained volume strongly affects the final topology and the iterative process. The optimization based on the stress-gradient instead does not involve an arbitrary choice and leads to results very similar to those obtained with the defect-distribution approach with V_{tot}. Differently from the defect-distribution approach, the stress-gradient methodology does not require any information about the defect size, which demands further investigations on the fracture surface of the tested specimens, as described in Section 3.1. As such, this methodology appears more suitable in industrial applications.
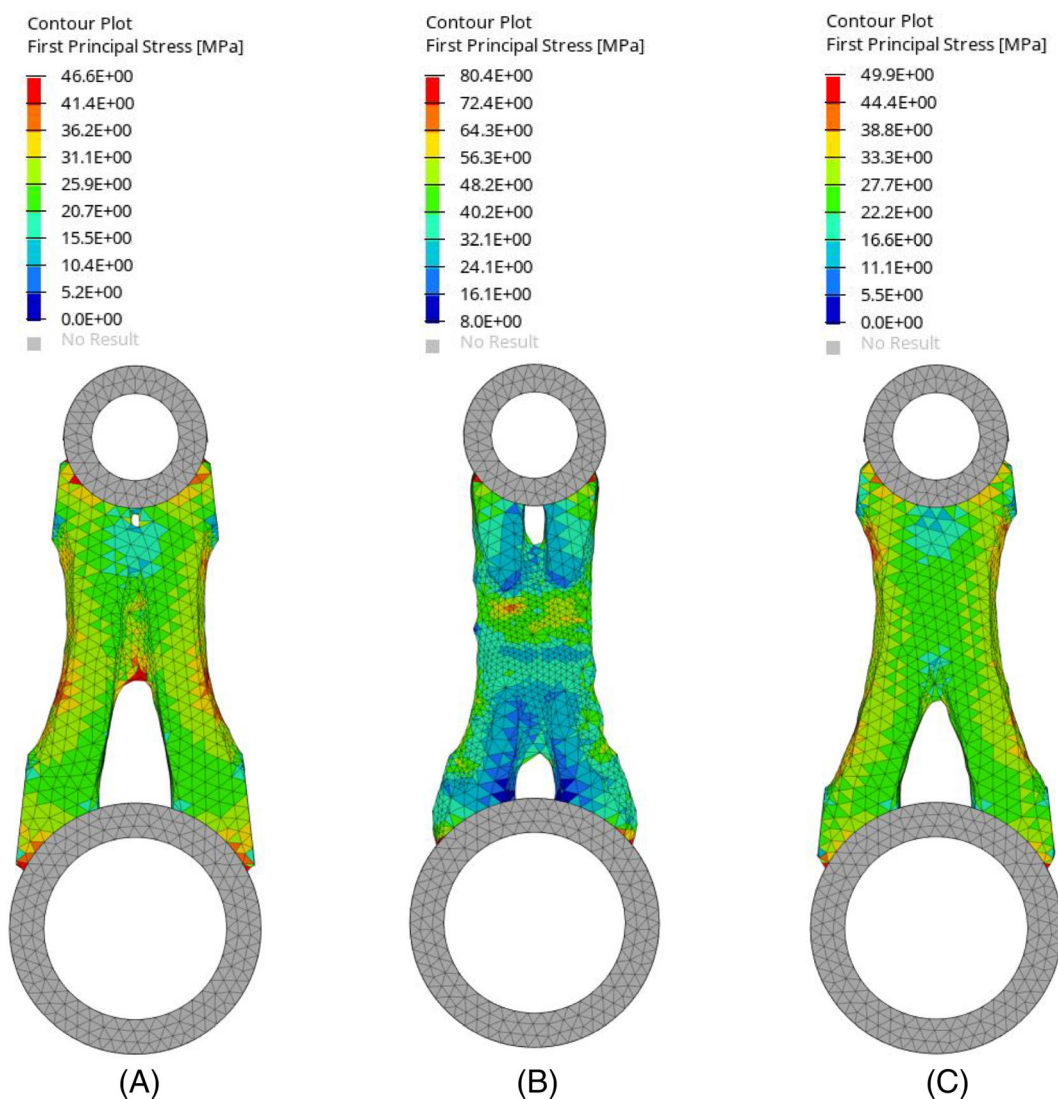

FIGURE 8 Topologies and contour plots of the first principal stress: (A) defect-distribution based optimization with fatigue constraint calculated on the total volume; (B) defect-distribution based optimization with fatigue constraint calculated on the V_{90}; (C) stress-gradient based optimization. [Colour figure can be viewed at wileyonlinelibrary.com]

Under static loading conditions, all the topologies sustain the load with remarkable discrepancy with respect to the ultimate strength of the material. For example, in the topology obtained with the defect-distribution approach with V_{90}, which is the less conservative structure, the maximum Von Mises stress is equal to 140 MPa, which is consistently smaller than the yield strength of the material, that is, 287 MPa.

4 | CONCLUSIONS

The present paper deals with TO algorithms against static and fatigue failures. Two methodologies, which model the fatigue response in the finite life range and account for the experimental scatter due to the presence of manufacturing defects, are compared. Defects generally originate during the manufacturing process, and their influence on the fatigue response cannot be neglected in structural applications, especially when dealing with TO designs, which are likely realized by AM. The first approach is based on the defect distribution and the marginal P-S-N curves resulting from experimental data and investigations of the critical defect size on the fracture surface. The second method models the size-effect, that is, the reduction of fatigue strength as the loaded volume increases, by considering the stress gradient within the loaded material. The dependency on the defect size is not made explicit in the method but is considered in the material parameters determined from the experimental data.

As the fatigue strength depends on the volume of the topology (defect-distribution method) or on the stress distribution (stress-gradient method), both methodologies require an iterative procedure to determine the optimal design. In particular, at the end of an optimization run, the fatigue strength is calculated from the resulting topology and compared to the value considered in the optimization process. If the discrepancy is lower than 1%, the convergence is met, and the optimal design is identified. On the contrary, if the discrepancy is higher than 1%, another optimization is performed with the updated fatigue strength. The methodology thus proceeds until convergence is reached.

The two approaches have thus been used to assess the maximum allowable first principal stress, which causes crack propagation in fatigue. The optimal topologies of a cantilever beam and of an engine rod subjected to static and fully reversed fatigue loads have then been determined by imposing the fatigue constraint in the fatigue loading condition and by limiting the Von Mises stress by the yield material strength in the static loading case. The parameters required by the methods have been determined from the experimental data obtained by the authors in previous work. The TOs have been performed in the *Hypermesh* environment.

Results have shown that the defect-distribution method that accounts for the whole volume V_{tot} of the topology at the end of the optimization run is the most conservative. Indeed, this approach assumes that the largest defect is equivalently present in all the elements of the FE model. However, the choice of the volume to consider at the end of the optimization run for the calculation of the updated fatigue strength is arbitrary and can lead to consistently different results, as shown by accounting only the V_{90}, that is, the volume of material subjected to at least 90% of the maximum stress amplitude, in the TO of the engine rod.

Results of the optimal design based on the stress-gradient method have shown that the fatigue strength calculated through this approach is strongly dependent on the stress distribution within the part. In the cantilever beam model, only a few elements, that is, sub-volumes of the component, experienced high stress levels, and a fatigue strength consistently higher than the conservative value obtained with the defect-distribution method was obtained. On the contrary, the stress field of the engine rod was more uniform, and the fatigue strength assessed with the stress-gradient method approximated the conservative value of the defect-distribution approach. Finally, it is worth noticing that the stress-gradient method does not require complex analyses of the fracture surface for the assessment of the critical defect size and therefore appears more suitable in industrial applications.

NOMENCLATURE

AM	Additive Manufacturing
TO	Topology Optimization
FE	Finite Element
LEVD	Largest Extreme Value Distribution
P-S-N curves	probabilistic S-N curves
Cdf	cumulative distribution function
Pdf	probability density function
N_f	number of cycles to failure
n	number of cycles
s_a	stress amplitude
$F_Y(y;x)$	cumulative distribution function of the fatigue life
μ_Y, σ_Y	mean and standard deviation of the fatigue life
$\sqrt{a_c}$	critical defect size
$f_{\sqrt{a_c}}$	probability density function of the defect size
$\mu_{\sqrt{A}}, \sigma_{\sqrt{A}}$	scale and location parameters of the LEVD distribution of the defect size

v_i	volume of the i-th element
s_i	first principal stress amplitude of the i-th element
s_{max}	maximum first principal stress amplitude within the component
s_1	first principal stress
s_{lim}	maximum allowable first principal stress amplitude
s_{eq}	Von Mises stress
s_y	yield strength of the material
$\overline{\overline{\rho}} = \{\rho_1, \rho_2, ..., \rho_{N_e}\}$	relative density of the N_e elements
$\overline{\overline{K}}$	stiffness matrix
$\overline{u}$	displacement vector
$\overline{F}$	external force vector
V_0	initial volume of the component
V_{opt}	optimal volume to obtain at the end of the TO
V_{90}	volume above the 90% of the maximum applied stress
C	compliance of the component
m	mass of the component

DATA AVAILABILITY STATEMENT

The data that support the findings of this study are available on request from the corresponding author. The data are not publicly available due to privacy or ethical restrictions.

ORCID

Carlo Boursier Niutta https://orcid.org/0000-0002-7894-4752

Andrea Tridello https://orcid.org/0000-0003-3007-3377

Davide S. Paolino https://orcid.org/0000-0002-4231-4580

REFERENCES

1. Wirsching PH. Probabilistic Fatigue Analysis. In: Sundararajan C, ed. *Probabilistic Structural Mechanics Handbook*. Springer; 1995:146-165. doi:10.1007/978-1-4615-1771-9_7

2. Hosseini ZS, Dadfarnia M, Somerday BP, Sofronis P, Ritchie RO. On the theoretical modeling of fatigue crack growth. *J Mech Phys Solids*. 2018;121:341-362.

3. Murakami Y. *Metal fatigue: effects of small defects and nonmetallic inclusions*. Elsevier Ltd; 2002.

4. Ingarao G, Priarone PC. A comparative assessment of energy demand and life cycle costs for additive- and subtractive-based manufacturing approaches. *J Manuf Process*. 2020;56:1219-1229.

5. Gao C, Wolff S, Wang S. Eco-friendly additive manufacturing of metals: energy efficiency and life cycle analysis. *J Manuf Syst*. 2021;60:459-472.

6. Bendsøe MP, Sigmund O. *Topology optimization*. Springer; 2002.

7. Beretta S, Romano S. A comparison of fatigue strength sensitivity to defects for materials manufactured by AM or traditional processes. *Int J Fatigue*. 2017;94:178-191.

8. Masuo H, Tanaka Y, Morokoshi S, et al. Influence of defects, surface roughness and HIP on the fatigue strength of Ti-6Al-4V manufactured by additive manufacturing. *Int J Fatigue*. 2018; 117:163-179.

9. Solberg K, Guan S, Razavi SMJ, Welo T, Chan KC, Berto F. Fatigue of additively manufactured 316L stainless steel: the influence of porosity and surface roughness. *Fatigue Fract Eng Mater Struct*. 2019;42(9):2043-2052.

10. Solberg K, Wan D, Berto F. Fatigue assessment of as-built and heat-treated Inconel 718 specimens produced by additive manufacturing including notch effects. *Fatigue Fract Eng Mater Struct*. 2020;43(10):2326-2336.

11. Yamashita Y, Murakami T, Mihara R, Okada M, Murakami Y. Defect Analysis and Fatigue Design Basis for Ni-based Superalloy 718 manufactured by Additive Manufacturing. In: *Procedia structural integrity*. Vol.7. Elsevier B.V.; 2017:11-18.

12. Sanaei N, Fatemi A. Defects in additive manufactured metals and their effect on fatigue performance: a state-of-the-art review. *Prog Mater Sci*. 2021;117:100724. Preprint at. doi:10.1016/j.pmatsci.2020.100724

13. Zhu J, Zhou H, Wang C, Zhou L, Yuan S, Zhang W. A review of topology optimization for additive manufacturing: status and challenges. *Chin J Aeronaut*. 2021;34(1):91-110.

14. Holmberg E, Torstenfelt B, Klarbring A. Fatigue constrained topology optimization. *Struct Multidiscipl Optim*. 2014;50(2):207-219.

15. Oest J, Lund E. Topology optimization with finite-life fatigue constraints. *Struct Multidiscipl Optim*. 2017;56(5):1045-1059.

16. Dagkolu A, Gokdag I, Yilmaz O. Design and additive manufacturing of a fatigue-critical aerospace part using topology optimization and L-PBF process. *Procedia Manuf*. 2020;54:238-243.

17. Romano S, Miccoli S, Beretta S. A new FE post-processor for probabilistic fatigue assessment in the presence of defects and its application to AM parts. *Int J Fatigue*. 2019;125:324-341.

18. Gao X, Caivano R, Tridello A, et al. Innovative formulation for topological fatigue optimisation based on material defects distribution and TopFat algorithm. *Int J Fatigue*. 2021;147:106176.

19. Caivano R, Tridello A, Barletta G, et al. Defect-driven topology optimisation: TopFat algorithm validation via 3D components re-design for real industrial applications. *Procedia Structural Integrity*. 2022;39:81-88.

20. Boursier Niutta C, Tridello A, Barletta G, et al. Defect-driven topology optimization for fatigue design of additive manufacturing structures: application on a real industrial aerospace component. *Eng Fail Anal*. 2022;142:106737.

21. Le VD, Pessard E, Morel F, Edy F. Interpretation of the fatigue anisotropy of additively manufactured TA6V alloys via a fracture mechanics approach. *Eng Fract Mech*. 2019;214:410-426.

22. Tridello A, Boursier Niutta C, Berto F, Qian G, Paolino DS. Fatigue failures from defects in additive manufactured components: a statistical methodology for the analysis of the

experimental results. *Fatigue Fract Eng Mater Struct*. 2021; 44(7):1944-1960.

23. Paolino DS, Tridello A, Chiandussi G, Rossetto M. S-N curves in the very-high-cycle fatigue regime: statistical modeling based on the hydrogen embrittlement consideration. *Fatigue Fract Eng Mater Struct*. 2016;39(11):1319-1336.

24. Tridello A, Paolino DS, Rossetto M. Ultrasonic VHCF tests on very large specimens with risk-volume up to 5000 mm3. *Applied Sciences*. 2020;10(7):2210.

25. Paolino DS. Very high cycle fatigue life and critical defect size: modeling of statistical size effects. *Fatigue Fract Eng Mater Struct*. 2021;44(5):1209-1224.

26. Tridello A, Fiocchi J, Biffi CA, Rossetto M, Tuissi A, Paolino DS. Size-effects affecting the fatigue response up to 109 cycles (VHCF) of SLM AlSi10Mg specimens produced in horizontal and vertical directions. *Int J Fatigue*. 2022;160: 106825.

27. Invernizzi S, Paolino D, Montagnoli F, Tridello A, Carpinteri A. Comparison between fractal and statistical approaches to model size effects in VHCF. *Metals (Basel)*. 2022; 12(9):1499.

28. AltairEngineering. https://support.altair.com/csm?id=altair_product_documentation. (2022).

29. Paolino DS, Tridello A, Chiandussi G, Rossetto M. On specimen design for size effect evaluation in ultrasonic gigacycle fatigue testing. *Fatigue Fract Eng Mater Struct*. 2014;37(5): 570-579.

30. Tridello A, Fiocchi J, Biffi CA, et al. VHCF response of Gaussian SLM AlSi10Mg specimens: effect of a stress relief heat treatment. *Int J Fatigue*. 2019;124:435-443.

31. Shenoy PS. *Dynamic Load Analysis and Optimization of Connecting Rods*. University of Toledo; 2004.

How to cite this article: Boursier Niutta C, Tridello A, Paolino DS. Fatigue design of Additive Manufacturing components through Topology Optimization: Comparison of methodologies based on the defect distribution and on the stress gradient. *Fatigue Fract Eng Mater Struct*. 2023;1-17. doi:10.1111/ffe.14082